Supplementary Information

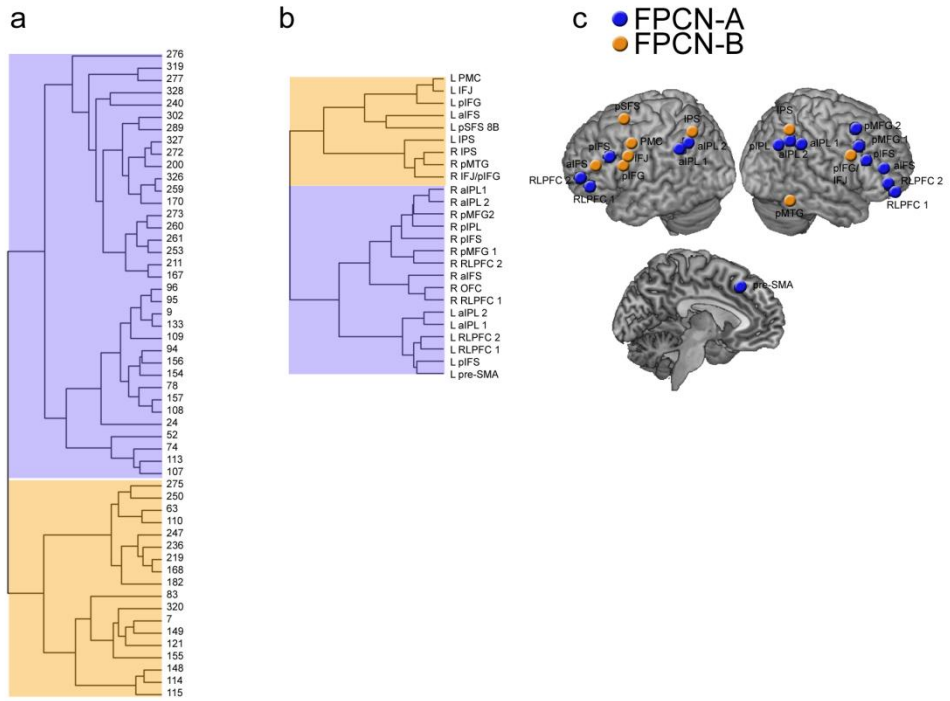

Figure 1. FPCN fractionation based on intra-modular connectivity. **(a)** Hierarchical clustering results based on intra-modular (within-FPCN) connections using Gordon parcellation nodes. Node number corresponds to the labelled ROI in the 333 node file available at: http://www.nil.wustl.edu/labs/petersen/Resources.html. **(b)** Hierarchical clustering results based on intra-modular connections using Power parcellation nodes. **(c)** Surface rendering of FPCN nodes from the Power parcellation, color-coded based on the hierarchical clustering results. Abbreviations: RLPFC, rostrolateral prefrontal cortex; pMFG, posterior middle frontal gyrus; aIPL, anterior inferior parietal lobule; pMTG, posterior middle temporal gyrus; pre-SMA, pre-supplementary motor area; aIFS, anterior inferior frontal sulcus; pIFS, posterior inferior frontal sulcus; IPS, intraparietal sulcus; pSFS, posterior superior frontal gyrus; pIFG, posterior inferior frontal gyrus; IFJ, inferior frontal junction; PMC, premotor cortex.

.

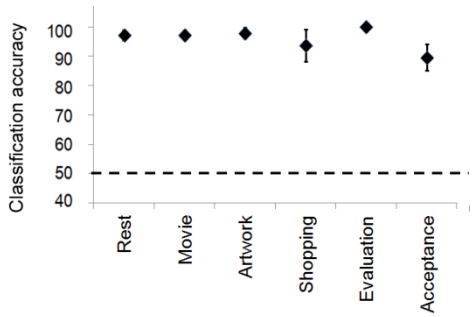

Figure 2. Classifier accuracy in distinguishing $FPCN_A$ and $FPCN_B$ FC patterns based on intra-modular connections using an ANOVA kernel. Error bars reflect between subject SEM.

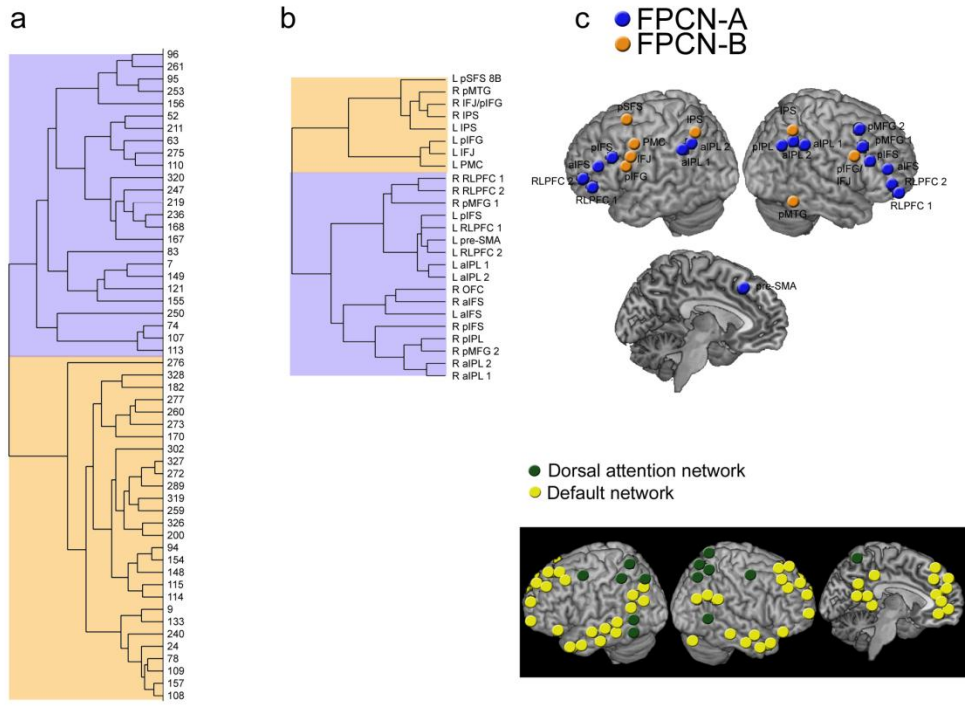

Figure 3. FPCN fractionation based on inter-network connectivity. **(a)** Hierarchical clustering of FPCN nodes based on FC with the DN and DAN using Gordon parcellation nodes. Node number corresponds to the labelled ROI in the 333 node file available at: http://www.nil.wustl.edu/labs/petersen/Resources.html. **(b)** Hierarchical clustering results based on Power parcellation nodes. **(c)** Surface rendering of FPCN nodes from the Power parcellation, color-coded based on the hierarchical clustering results. Abbreviations: RLPFC, rostrolateral prefrontal cortex; pMFG, posterior middle frontal gyrus; aIPL, anterior inferior parietal lobule; pMTG, posterior middle temporal gyrus; pre-SMA, pre-supplementary motor area; aIFS, anterior inferior frontal sulcus; pIFS, posterior inferior frontal sulcus; IPS,

intraparietal sulcus; pSFS, posterior superior frontal gyrus; pIFG, posterior inferior frontal gyrus; IFJ, inferior frontal junction; PMC, premotor cortex.

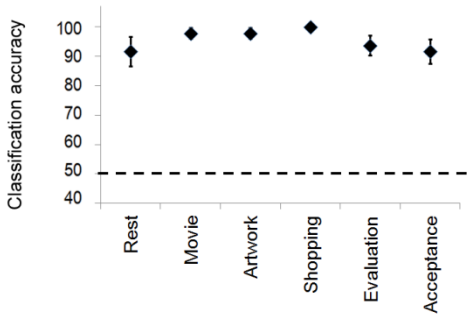

Figure 4. Classifier accuracy in distinguishing $FPCN_A$ and $FPCN_B$ FC patterns based on inter-modular connections with the DN and DAN using an ANOVA kernel. Error bars reflect between subject SEM.

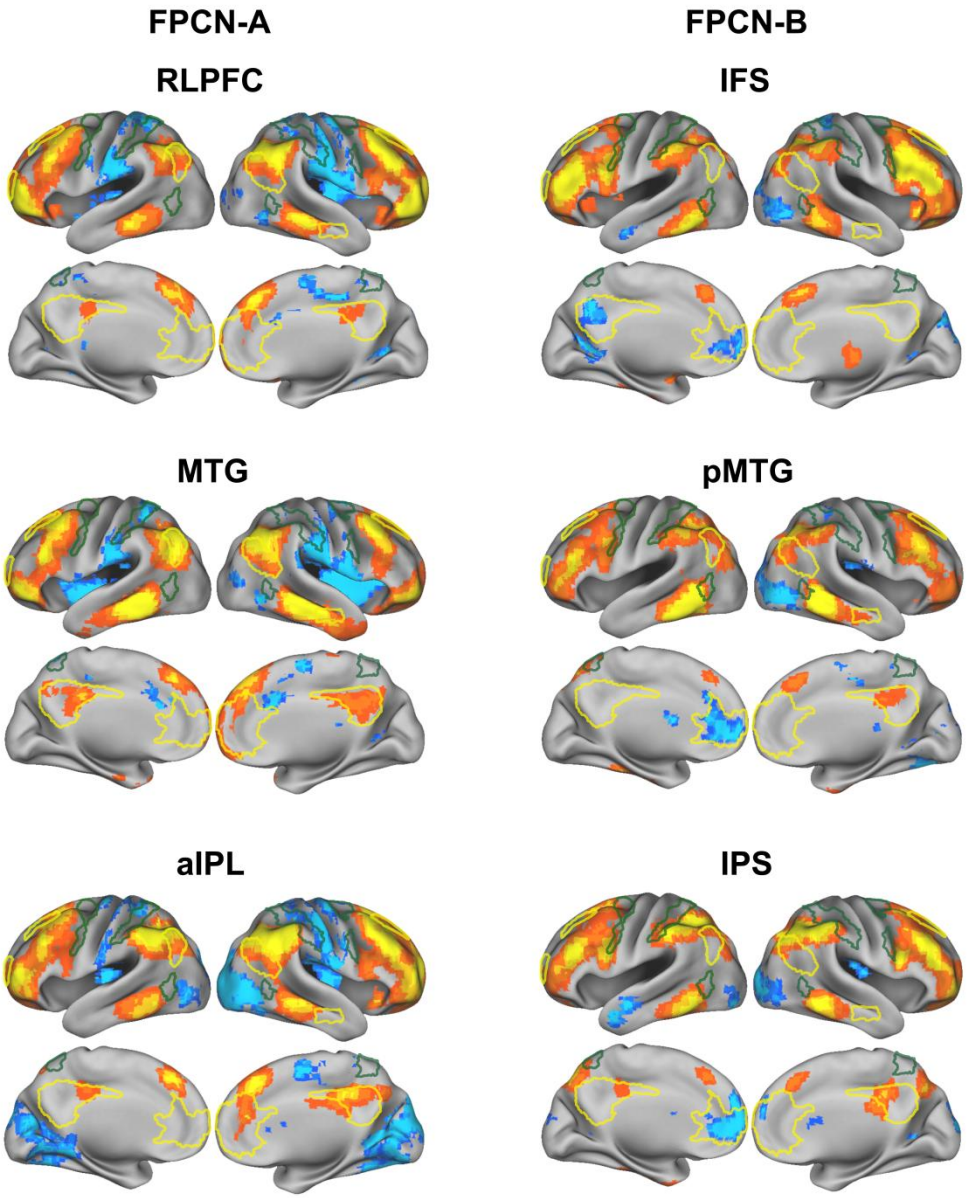
FPCN-A
RLPFC
FPCN-B
IFS
MTG
pMTG
aIPL
IPS

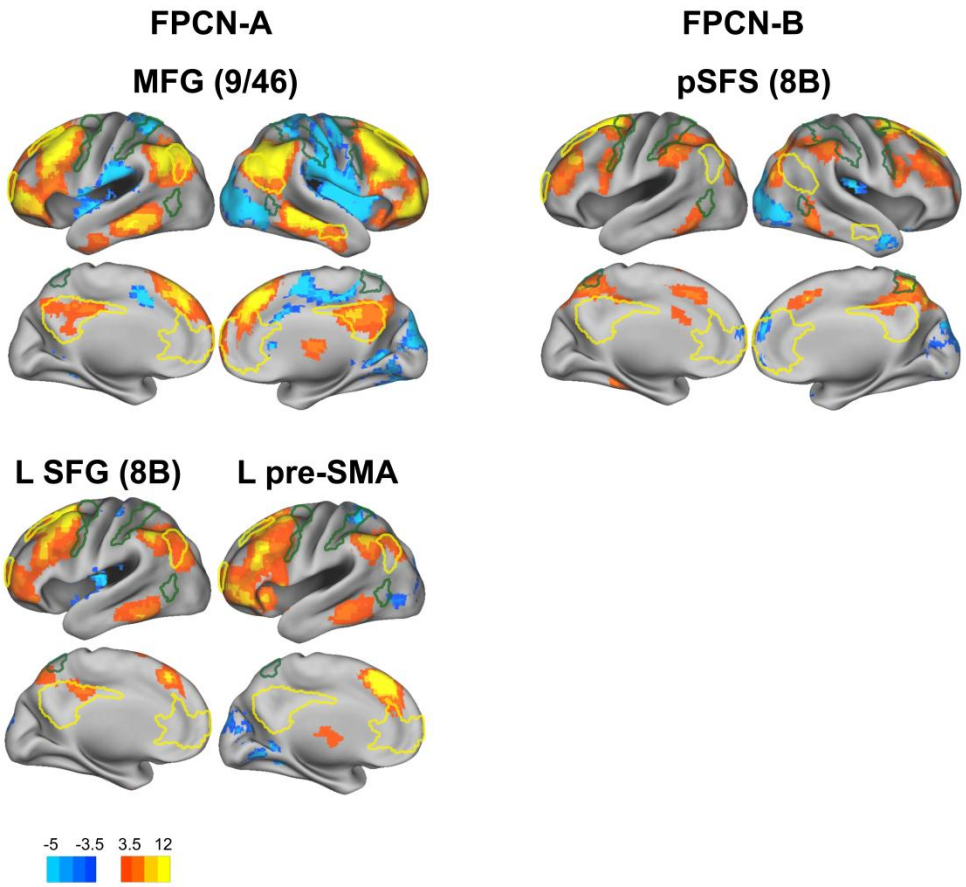

Figure 5. Seed-based voxel analysis. We computed seed-based functional connectivity (FC) maps for $FPCN_A$ and $FPCN_B$ seed regions from the Yeo parcellation in order to examine the spatial topography of positively and negatively correlated voxels with the rest of the brain. The timeseries of all voxels within each ROI were averaged, and first-level correlation maps were produced by computing the Pearson correlation between that seed timeseries and the timeseries of all other voxels. Correlation coefficients were converted to normally distributed Fisher transformed *z*-scores to allow for second-level GLM analyses. To correct for multiple comparisons, we used a combined height and cluster threshold ($Z > 3.1$, $p < .05$ FWE cluster corrected). Results were visualized with CARET brain mapping software (http://brainmap.wustl.edu/caret). We examined the location of positively and negatively correlated voxels in relation to the DN (yellow borders) and DAN (green borders) network boundaries from the Yeo 17-network parcellation. Abbreviations: RLPFC, rostrolateral prefrontal cortex; MFG, middle frontal gyrus; aIPL, anterior inferior parietal lobule; pMTG, posterior middle temporal gyrus; pre-SMA, pre-supplementary motor area; IFS, inferior frontal sulcus; IPS, intraparietal sulcus; pSFS, posterior superior frontal gyrus; SFG, Superior frontal gyrus.

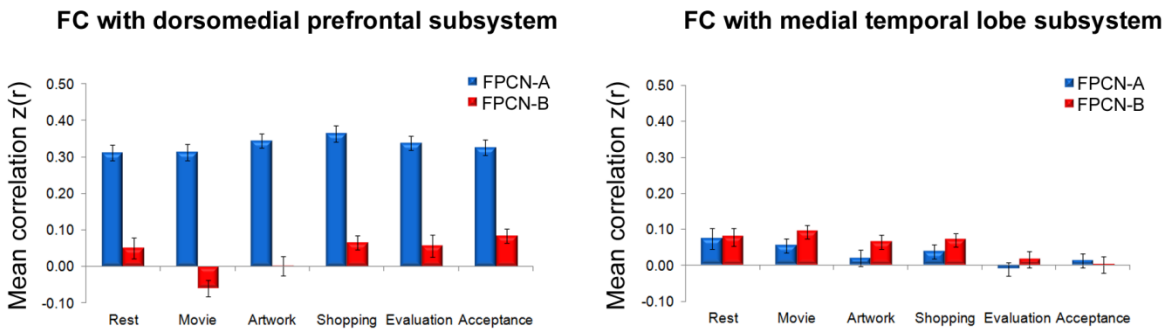

Figure 6. FPCN FC patterns with the dorsomedial prefrontal and medial temporal lobe subsystems of the DN based on the Yeo 17-network parcellation. Error bars reflect between subject SEM.

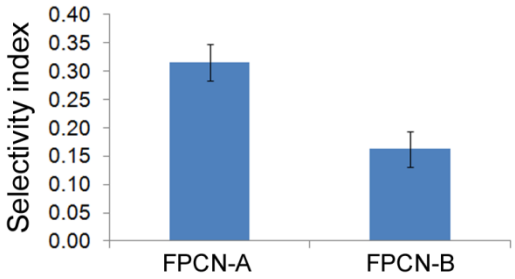

Figure 7. Mean node selectivity. The "selectivity index" was computed for each FPCN node as mean FC with DN nodes minus mean FC with DAN nodes. We then averaged across values for all $FPCN_A$ nodes and all $FPCN_B$ nodes. In the case of $FPCN_B$ nodes, the values were first multiplied by -1 such that they reflected greater FC with the DAN relative to the DN. This was done for each condition in the primary data set separately, and then we computed the average "selectivity index" across conditions. The "selectivity index" was computed for each participant, and then averaged across participants. Error bars reflect between subject SEM.

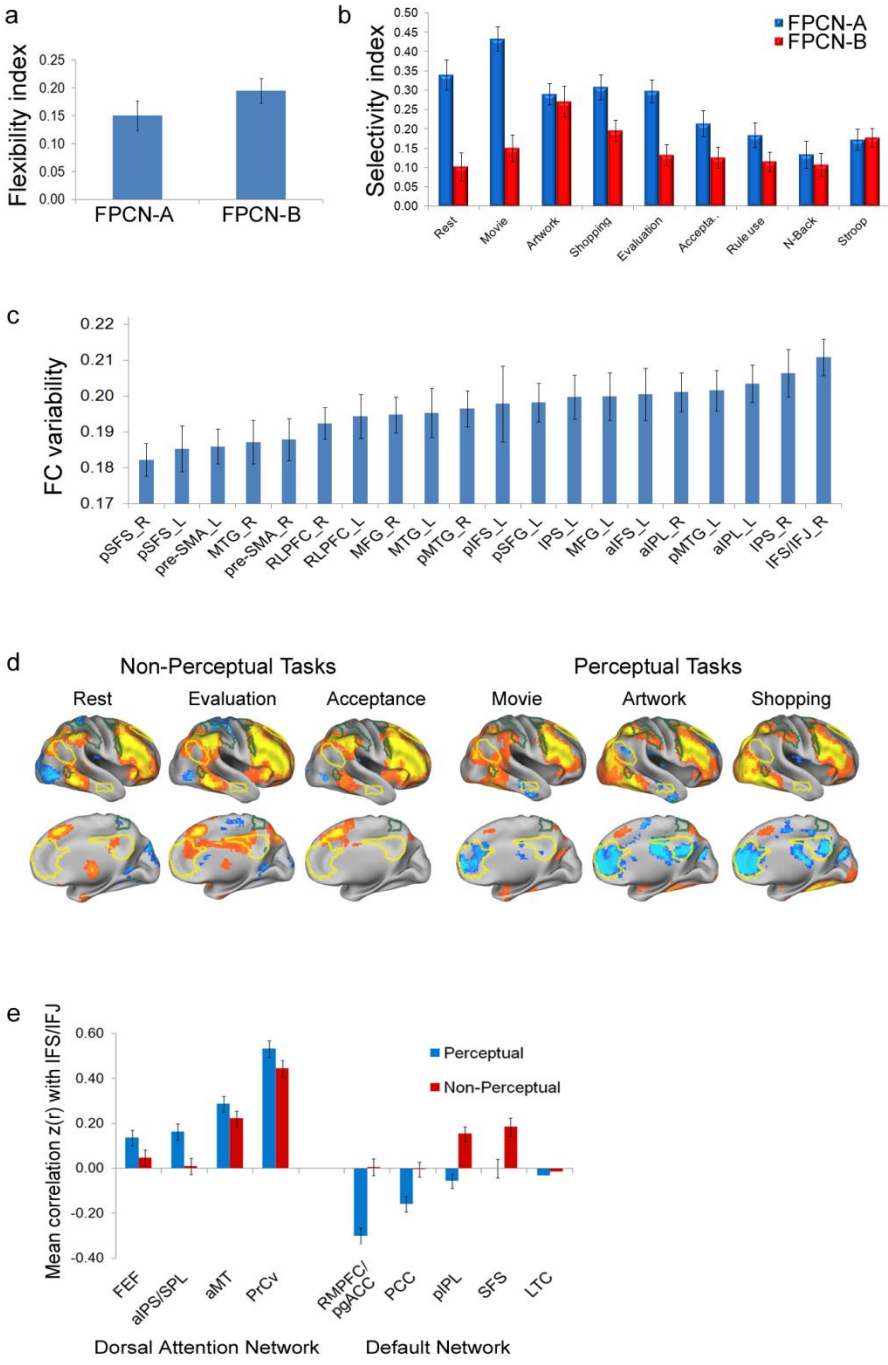

Figure 8. Task-related flexibility of functional connectivity patterns**. (a)** Flexibility index reflecting the extent to which FC with the DN and DAN changes across contexts, using the Yeo parcellation nodes. Both the $FPCN_A$ and $FPCN_B$ exhibit significant flexibility, but the effect is stronger for the $FPCN_B$. **(b)** The "selectivity index" varies in strength across conditions for both FPCN subsystems. Interestingly, the "selectivity index" is stronger during the conditions with perceptual demands (movie, artwork, and shopping) compared to the conditions that do not involve a perceptual component (rest, evaluation-based introspection, and acceptance-based introspection) and this was the case for both FPCN-A (paired t-test: $p = .003$) and FPCN-B (paired t-test: $p = .002$). **(c)** Variability of FC with the DN and DAN across conditions for each FPCN node. Values reflect mean variability (SD) of FC across conditions

between each FPCN node and DN and DAN nodes. The IFS/IFJ ROI exhibited the greatest FC flexibility across conditions. **(d)** IFS/IFJ seed maps for each condition. For illustration purposes, we use a slightly liberal threshold to show the full extent of positively and negatively correlated voxels ($Z > 2.57$, $p < .05$ FDR cluster corrected). **(e)** Mean FC between the IFS/IFJ and DN and DAN nodes during perceptual and non-perceptual task conditions, showing flexible task-dependent coupling patterns. The IFS/IFJ encodes task demands[5,56] and contributes to the top-down control of attention[53] via shifting coupling patterns with different regions based on the target of attention[57]. This region may thus play an important role in coordinating DN and DAN processing based on current goals. Error bars reflect between subject SEM.

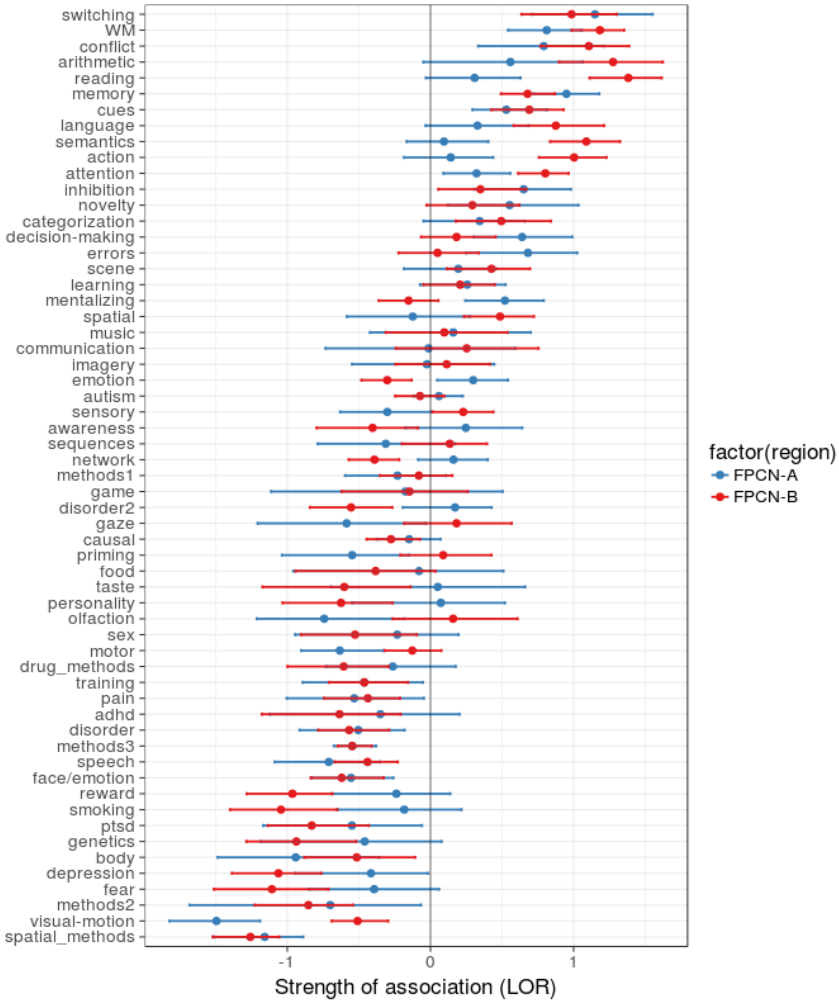

Figure 9. Meta-analytic functional preference profile of FPCN subsystems. We trained naïve Bayes classifiers to predict the presence or absence of activation in each FPCN subsystem using a set of 60 psychological topics and plotted topics that were significantly positively associated with at least one subsystem. Strength of association is measured in log odds-ratio (LOR) with values greater than 0 indicating that the presence of that topic in a study positively predicts activity in a subsystem. Ninety-five percent confidence intervals derived using bootstrapping are indicated.

Supplementary Results

Control for node distance. In many cases $FPCN_A$ nodes are spatially proximate to DN nodes, whereas $FPCN_B$ nodes are spatially proximate to DAN nodes. As such, differential coupling patterns could result from spatial smoothing which may increase coupling strength between adjacent regions. We conducted a control analysis to rule out the possibility that this could explain our results. We computed the average correlation between the rostrolateral prefrontal cortex (RLPFC)—a node within the $FPCN_A$—and several DN regions including the posterior cingulate cortex (PCC), posterior inferior parietal lobule (pIPL), superior frontal sulcus (SFS), and lateral temporal cortex (LTC), and compared this to the average correlation between the inferior frontal sulcus (IFS)—a node within the $FPCN_B$ —and these same regions. The IFS is spatially closer to these DN regions, so it should exhibit stronger FC with these regions if our results are mainly driven by spatial proximity. However, this was not the case. RLPFC coupling with these DN regions [mean $z(r)$ = .33] was much stronger than IFS coupling with these regions [mean $z(r)$ = .05], a difference that was statistically significant ($p < .001$). We also computed the average correlation between the middle temporal gyrus (MTG)—a node within the $FPCN_A$—and several DAN regions including the frontal eye fields and ventral precentral cortex, and compared this to the average correlation between the posterior middle temporal gyrus (pMTG)—a node within the $FPCN_B$ —and these same regions. In this case, the MTG is spatially closer to these DAN regions, so it should exhibit stronger FC with these regions if our results are mainly driven by spatial proximity. However, this was not the case. MTG coupling with these DAN regions [mean $z(r)$ = -.01] was much weaker than pMTG coupling with these regions [mean $z(r)$ = .11], a difference that was statistically significant ($p < .001$). Thus, the $FPCN_A$ exhibits stronger coupling with the DN and the $FPCN_B$ exhibits stronger coupling with the DAN even when spatial proximity of nodes cannot be a factor.

Control for motion. It is important to rule out the possibility that the relationship between dynamic FC interactions and network clustering could be explained by participant motion. We examined this in our primary data set. We examined total motion and framewise displacement. We computed the average amount of motion in each window, just as with between-network FC, and then computed the correlation between changes across time in motion and changes across time in between-network FC and clustering. These values were Fisher-transformed and submitted to a one-sample *t*-test to assess statistical significance at the group level, with $p = .004$ corresponding to $p < .05$ Bonferroni corrected for multiple comparisons. Notably, within each of the six contexts, temporal variation in the strength of between-network FC and temporal variation in the strength of clustering were uncorrelated with temporal variation in participant motion. We found no significant relationships at the group level in any context between motion and between-network FC [all: $|z(r)$'s$| < .09$, p's $> .05$, FWE corrected], or between motion and mean weighted clustering [all: $|z(r)$'s$| < .12$, p's $> .05$, FWE corrected]. There was also no evidence of systematic relationships at the level of individual participants. For between-network FC we found that 19 out of 284 correlations (~ 7%) were significantly positive at $p < .05$,

Bonferroni corrected, and 22 out of 284 correlations (~ 8%) were significantly negative at $p < .05$, Bonferroni corrected. For clustering, we found that 33 out of 284 correlations (~ 12%) were significantly positive at $p < .05$, Bonferroni corrected, and 39 out of 284 correlations (~ 14%) were significantly negative at $p < .05$, Bonferroni corrected. Thus, while some participants did show significant correlations with motion in some contexts, this was rare, and the correlations were not systematically positive or negative. Thus, the observed time-dependent relationships between network interactions and clustering strength cannot be explained by participant motion.